Received: 22 February 2019 | Revised: 21 September 2019 | Accepted: 1 October 2019

DOI: 10.1002/joc.6343

RESEARCH ARTICLE

International Journal of Climatology RMetS

Power-law behaviour of hourly precipitation intensity and dry spell duration over the United States

Lichao Yang[1,2] | **Christian L. E. Franzke**[2,3] | **Zuntao Fu**[1]

[1]Lab for Climate and Ocean-Atmosphere Studies, Department of Atmospheric and Oceanic Sciences, School of Physics, Peking University, Beijing, China

[2]Center for Earth System Research and Sustainability, University of Hamburg, Hamburg, Germany

[3]Meteorological Institute, University of Hamburg, Hamburg, Germany

Correspondence
Zuntao Fu, Lab for Climate and Ocean-Atmosphere Studies, Department of Atmospheric and Oceanic Sciences, School of Physics, Peking University, Beijing, China.
Email: fuzt@pku.edu.cn

Funding information
National Natural Science Foundation of China, Grant/Award Numbers: 41475048, 41675049; Deutsche Forschungsgemeinschaft (DFG German research Foundation), Grant/Award Number: 274762653

Abstract

Precipitation is an important meteorological variable which is critical for weather risk assessment. For instance, intense but short precipitation events can lead to flash floods and landslides. Most statistical modelling studies assume that the occurrence of precipitation events is based on a Poisson process with exponentially distributed waiting times while precipitation intensities are typically described by a gamma distribution or a mixture of two exponential distributions. Here, we show by using hourly precipitation data over the United Sates that the waiting time between precipitation events is non-exponentially distributed and best described by a fractional Poisson process. A systematic model selection procedure reveals that the hourly precipitation intensities are best represented by a two-distribution model for about 90% of all stations. The two-distribution model consists of (a) a generalized Pareto distribution (GPD) model for bulk precipitation event sizes and (b) a power-law distribution for large and extreme events. Finally, we analyse regional climate model output to evaluate how the climate models represent the high-frequency temporal structure of U.S. precipitation. Our results reveal that these regional climate models fail to accurately reproduce the power-law behaviour of intensities and severely underestimate the long durations between events.

KEYWORDS

extreme precipitation, hourly precipitation, power-law distribution, regional climate model, waiting time distribution

1 | INTRODUCTION

Precipitation plays an important part in the global water cycle and is of utmost socio-economic relevance. More and more studies are focusing on the analysis of high-frequency precipitation since it is more sensitive to climate change (Berg *et al*., 2013; Muschinski and Katz, 2013). Flash floods, landslides and hydrological processes that control the surface and subsurface water distribution mostly depend on sub-daily precipitation. For instance, the flooding in Boscastle, southwest England, in August 2004 was caused by heavy rain which fell over a 5-hr period (Wheater, 2006). Furthermore, groundwater-levels can have rapid responses to precipitation which falls over periods of less than 2 hr (Cai and Ofterdinger, 2016). Therefore, a good understanding of precipitation on finer temporal resolutions is necessary and will be essential for watershed hydrology, natural hazard assessment and hydrological process predictions of climate change.

There are two main approaches to understanding and modelling of high-frequency precipitation. One is using regional climate models, while the other is using stochastic precipitation models, also called weather generators (e.g., Liang *et al*., 2004; Paschalis *et al*., 2013). Regional climate models, which resolve the physical and dynamical processes better than global GCMs, are able to represent precipitation on higher spatial and temporal resolutions (Evans, 2011). Climate models

should ideally be able to reproduce accurately the statistical properties of local-scale observations (Maraun *et al*., 2010). However, precipitation is one of the variables most sensitive to model formulation and strongly dependent on the parameterization scheme. Even though regional climate models have skill in capturing the statistics of daily precipitation sums, they cannot represent well sub-daily precipitation (Lenderink and Van Meijgaard, 2008). Biases still exist in model simulations so that a quantitative assessment is necessary before they can be used for policy decision support (Martynov *et al*., 2013; Haerter *et al*., 2015).

Stochastic precipitation models aim to generate surrogate time series, resembling the statistical properties of the observed temporal and spatial structures of precipitation. A key aspect is how to characterize the precipitation event and inter-event occurrences. Some are based on a Poisson process, which is able to generate the presence of wet and dry spells (Rodriguez-Iturbe *et al*., 1987; Onof *et al*., 2000). To be more specific, some assume that the waiting time of precipitation storm arrivals and storm durations is following a Poisson process, which means that precipitation events are independent events and the waiting time between events is exponentially distributed. However, recent studies found that the standard Poisson process is not able to represent the heavy tail of waiting times of precipitation events (Bernardara *et al*., 2007). Other stochastic precipitation models are based on first-order or higher-order Markov chain models, assuming the probability of precipitation on any day depends only on the previous day, for first-order Markov models, or on several past days, for higher-order Markov models (Woolhiser *et al*., 1982). However, these Markov models generate too few long dry spells and too few extreme events when compared to observations (Lennartsson *et al*., 2008; Hannachi, 2014). Another alternative stochastic precipitation model is the two-state renewal process. In this model, the waiting time distribution is based on some distributions, including truncated negative binomial distribution (Woolhiser *et al*., 1982) and the generalized Pareto distribution (GPD, Salvadori and De Michele, 2001). However, also this model cannot reproduce the observations accurately. Hence, an improved understanding and modelling of precipitation event arrival times are needed.

How to model the intensity of precipitation is an intricate topic, due to the complex temporal structures of precipitation. Some studies assume that the daily precipitation intensity is distributed according to a Gamma (Buishand, 1978), mixed exponential (Wilks and Wilby, 1999) which are light-tailed or heavy-tailed distributions (Mielke and Johnson, 1974; Papalexiou *et al*., 2013) such as a log-normal (Swift Jr and Schreuder, 1981) or a stretched exponential (Wilson and Toumi, 2005) distribution. Even though a good weather generator should present well the distribution of the whole intensity range, selecting the model for heavy precipitation plays a more important role for certain applications, since heavy precipitation has a higher impact on people's lives and is more likely to be influenced by global warming (Lenderink and Van Meijgaard, 2008). Hence, how the distribution of heavy precipitation decays is an important topic and widely studied. Cavanaugh *et al*. (2015) examined over 22,000 weather stations globally and found that heavy daily precipitation sums are power-law distributed. Olsson and Burlando (2002) found that the larger intermittent fluctuations of precipitation and the scaling property of precipitation lead to a power-law distribution for the extremes. Another possible model for the power-law range of precipitation is the idea of self-organized criticality (Bak *et al*., 1988; Peters *et al*., 2001). In such a process the event intensity is power-law distributed until it reaches an exponential cut-off for large events (Martinez-Villalobos and Neelin, 2018).

Recently, Papalexiou (2018) proposed a unified theory for stochastic modelling of hydroclimatic processes and used generalized Gamma (GenGam) and Burr Type XII (BurrXII) distributions to preserve the marginal distribution of precipitation intensities. He found that the exponential tails are severely underestimating the magnitudes of the extremes. Papalexiou *et al*. (2018) also compared power-law and stretched exponential tail fits and found the latter performs better. Therefore, selecting and evaluating the probability distribution for precipitation intensity, especially for large events, is still an important topic and needs to be better understood.

Here we aim to address the following research questions: (a) What is the optimal waiting time distribution for hourly precipitation events? (b) How best to model the intensity distribution of hourly precipitation? and (c) How well do regional climate models reproduce the hourly precipitation observations? Our study will provide the building blocks of a statistical generator for hourly precipitation from a new perspective. In Section 2 we describe the used observational and regional climate mode data sets and the statistical methods. In Section 3 we present our results of the analysis of the observational data and their comparison with the regional climate simulations. In Section 4 we discuss the physical insights of power-law behaviour of our results. In Section 5 we conclude our study.

2 | DATA AND METHODS

We use 110 hourly instrumental precipitation data records for the period 2008–2017 across the United States, provided by the U.S. Climate Reference Network program (USCRN). The data set can be obtained from the website https://www.ncdc.noaa.gov/crn/. Even though there are only 110 stations with 10 years of data, the USCRN precipitation records are of high quality, with a minimum measurement level of 0.2 mm and an accuracy of 0.1 mm. Compared with other hourly precipitation records (TD3240; [https://www1.ncdc.noaa.gov/pub/data/cdo/documentation/PRECIP_HLY_documentation.pdf]),

it can provide more reliable and broader intensity ranges (see Appendix for details). Following previous studies (e.g., Peters *et al*., 2001), a precipitation event is defined as a sequence of consecutive hourly precipitation observations with a rain rate greater than a threshold of zero; due to the minimum measurement level, we define rain events to have at least an amount of 0.2 mm. The waiting time is the interval between consecutive rain events, also called dry spells. The missing values in the observational time series take up less than 1%. When a rain event or a dry spell is interrupted by missing data, we discarded the corresponding event or non-rain period. We also checked the robustness of our results in the case that we replace the missing values with linear interpolation and with zeros (not shown). Sensitivity tests show that our results are not sensitive to how we treat the missing values. Here we focus on two seasons, respectively, summer (JJAS) and winter (NDJF), since heavy precipitation events are more likely to occur in summer and dry spells more in winter (Hitchens *et al*., 2013).

For comparison with regional climate models, we used the following global and regional climate model combinations: Canadian Earth System Model (CanESM2) downscaled by CanRCM4 (CanESM2-CanRCM4), Max Planck Institute Earth System Model (MPI) downscaled by RegCM4 (MPI-RegCM4) and Geophysical Fluid Dynamics Laboratory Earth System Model (GFDL) downscaled by WRF (GFDL-WRF). The regional climate simulations are collected by the Coordinated Regional Climate Downscaling Experiment program (CORDEX). For all three models we selected the Representative Concentration Pathway 8.5 (RCP85) emissions scenario simulations since these overlap with the observation period 2008–2017. The results of RCP45 are similar to RCP85 for the considered time period (not shown). These regional models produced hourly precipitation time series on grids of 0.44° resolution. Specific information of the models can be found at http://na-cordex.org. The same definition of precipitation event intensity and waiting time is also applied to the model output.

The station observations remain the most reliable and primary source of information for the historical precipitation. They also avoid introducing potential errors from the interpolation and data assimilation process. Generally, the evaluation between model simulations and station observations is difficult because station observations are point values, while the model simulations provide values representing the area of a grid box. Such a scale mismatch is especially obvious for global climate models and coarse resolution reanalysis. Here we use high-resolution regional climate model simulations and it has been shown that regional climate model simulations provide more realistic information of precipitation, with intensities and frequencies comparable to the recorded station data (Chan *et al*., 2013), than global climate models. To make a direct comparison between station data and model simulations, some studies remap the gauge measurements onto a regular grid similar to the simulations (Diaconescu *et al*., 2016), some interpolate the model grid points to the gauge locations (Xie *et al*., 2019), and some directly choose the grid points closest to the stations (Diaconescu *et al*., 2018; Pendergrass and Knutti, 2018). Here we choose the simplest way, in that we selected the closest grid point to compare with station observations.

To examine the event waiting time distribution, we use a Fractional Poisson process (FPP) (Laskin, 2003, 2009; Blender *et al*., 2015). The FPP is able to describe non-exponentially distributed waiting times, in particular power-law waiting times. The deviation from a standard Poisson process is described by the parameter ν. The waiting time density $\psi_{\nu,\mu}(t)$ of a fractional Poisson process is given by

$$\psi_{\nu,\mu}(t)=\mu t^{\nu-1}E_{\nu,\nu}(-\mu t^{\nu}), \tag{1}$$

where $\nu \in (0, 1]$ is the fractional exponent, μ is the intensity rate and $E_{\alpha,\beta}(z)=\sum_{n=0}^{\infty}\frac{z^n}{\alpha n+\beta}$ is the Mittag–Leffler function (Saxena *et al*., 2002). Figure 1 shows the FPP waiting time densities for different ν with $\mu = 0.1$. When $\nu = 1$, the waiting time simplifies to the standard Poisson process, which is exponentially distributed. When $\nu < 1$, the FPP exhibits power-law distributed waiting times. The lower ν is, the more the waiting time distribution is deviating from an exponential distribution, which leads to more short and long waiting times, but fewer medium ones. The estimation of the fractional parameter ν and μ is based on the method of moments (Cahoy *et al*., 2010).

To find the optimal model for the event intensity, here we focus more on selecting the appropriate distributions for the large events, since heavy precipitation has a higher-impact on people's lives. It is well known that precipitation is much more heavy tailed than an exponential distribution (Mielke and Johnson, 1974; Papalexiou *et al*., 2013). Many previous studies (Olsson and Burlando, 2002; Cavanaugh *et al*., 2015) have claimed that the tail of precipitation is power-law distributed, which is

$$P(X > x) \sim x^{-\alpha}, x > x_{\min}. \tag{2}$$

The detection of power-law distributions is of great importance since its extremes will be more frequent and more severe, compared with an exponential distribution. The most widely used method for identifying power-law behaviour is the one based on least-square fitting in a double-logarithmic plot. The starting point of linear fitting is defined as $x_{\min}$. The slope of the least-square fitting corresponds to α and low values of the residual sum of the squared errors are taken as evidence in favour of the power-law form. However, how to determine the starting point of linear fitting is a subjective

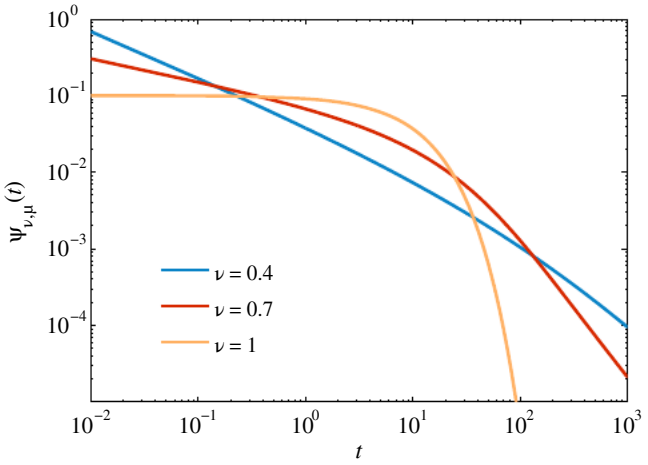

FIGURE 1 Waiting time density distributions of the fractional Poisson process (FPP) with $\nu = 0.4$, 0.7 and 1 and $\mu = 0.1$ [Colour figure can be viewed at wileyonlinelibrary.com]

procedure in this approach and the limited extreme samples obtained from exponential or other distributions can also lead to straight lines in double-log coordinates (Clauset *et al*., 2009). So appropriate methods are needed in order to define the power-law distributions in data. Here we apply the method proposed by Clauset *et al*. (2009) to distinguish the power-law from other distributions. According to their method, the two parameters, α and $x_{\min}$, are estimated by maximum log-likelihood estimation (MLE) and minimization of the Kolmogorov–Smirnov (K–S) statistics, respectively. One thing we want to point out here is that other distributions, such as the BurrXII and GPD can also provide power-law tails. But Equation (2) is the simplest form and we can get more specific information, such as when the power-law decay starts and its corresponding decay rate. For the bulk precipitation, we use a flexible model, the GPD. The distribution of the whole intensity x is,

$$f(x)=\begin{cases} f_{\mathrm{GP}}(x;\kappa,\sigma,\theta) & if \quad x<x_{\min} \\ f_{\mathrm{PL}}(x;\alpha) & if \quad x>x_{\min} \end{cases}, \tag{3}$$

where $f_{\mathrm{GP}}(x;\kappa,\ \sigma,\ \theta)$ is the generalized Pareto density with shape parameter κ, scale parameter σ and location parameter θ. $f_{\mathrm{PL}}(x;\alpha)$ is the power-law density and α is the slope of the power-law, also called scaling parameter. The two distributions are connected at x = $x_{\min}$. The $x_{\min}$ is the lowest bound of the power-law tail. All these parameters are estimated by maximum likelihood estimation (Clauset *et al*., 2009).

We use the Akaike Information Criterion (AIC) and Bayesian Information Criterion (BIC) to compare the combination of Power-law and GPD with many classic distributions, including exponential, generalized Pareto distribution, log-normal and the gamma distribution. Other various combinations of distributions are also compared such as a mixture of two exponential distributions and a power-law distribution until an exponential cut-off for large events which have been widely applied to simulate precipitation intensity surrogate time series (Wilks and Wilby, 1999; Bernardara *et al*., 2007; Paschalis *et al*., 2013; Martinez-Villalobos and Neelin, 2018). According to their criteria, we will choose the model that minimizes,

$$\mathrm{AIC}=2*k-2*\log\left(\hat{L}\right) \quad or \quad \mathrm{BIC}=k*\log(n)-2*\log\left(\hat{L}\right), \tag{4}$$

where k is the number of parameters in the model, n is the length of the time series and $\hat{L}$ is the maximum value of the likelihood function of the model.

We also compare the fitting with the BurrXII and GenGam distributions, since these two distributions are regarded as the unified model for daily precipitation (Papalexiou, 2018). Each of them contains one scale parameter (β) and two shape parameters (γ_1, γ_2) which control the left and right tail. The parameters of BurrXII and GenGam distributions are estimated by the L-moments method (Papalexiou and Koutsoyiannis, 2016). Both distributions have their limiting cases (Shao, 2004). A useful tool for identifying whether the distribution is suitable for the variable is the L-moments ratio diagram. The diagram provides a comparison between the statistics calculated from the records and the theoretical area (L-area) emerging from the distribution function. Here we apply the L-skewness versus the L-variation diagram and if the calculated statistics fall into the theoretical area, it means it can be fitted by the distribution (Papalexiou and Koutsoyiannis, 2016). Then two error measures are applied to compare the goodness of fit of the distributions (Papalexiou and Koutsoyiannis, 2016):

$$\mathrm{ER\text{-}I}=\frac{1}{n}\sum_{i=1}^{n}|\Delta x_i|, \tag{5}$$

$$\mathrm{ER\text{-}II}=\frac{x_{99}}{\hat{x}_{99}}, \tag{6}$$

where $\Delta x_i = x_i - \hat{x}_i$, x_i is estimated by the quantile function $x_i = Q_X(i)$, i = 10%, 11%, … 98% of the predicted intensities X, and $\hat{x}_i$ is the corresponding observed one. Thus, ER-I can provide an evaluation of the whole intensity range and ER-II focuses more on the extreme values. The best model will get the minimum ER-I and ER-II closest to 1.

3 | RESULTS

3.1 | Observational analysis

3.1.1 | Waiting time results

In order to better illustrate our results, we first focus on one station, Versailles in Kentucky (84.75 W, 38.09 N), to show

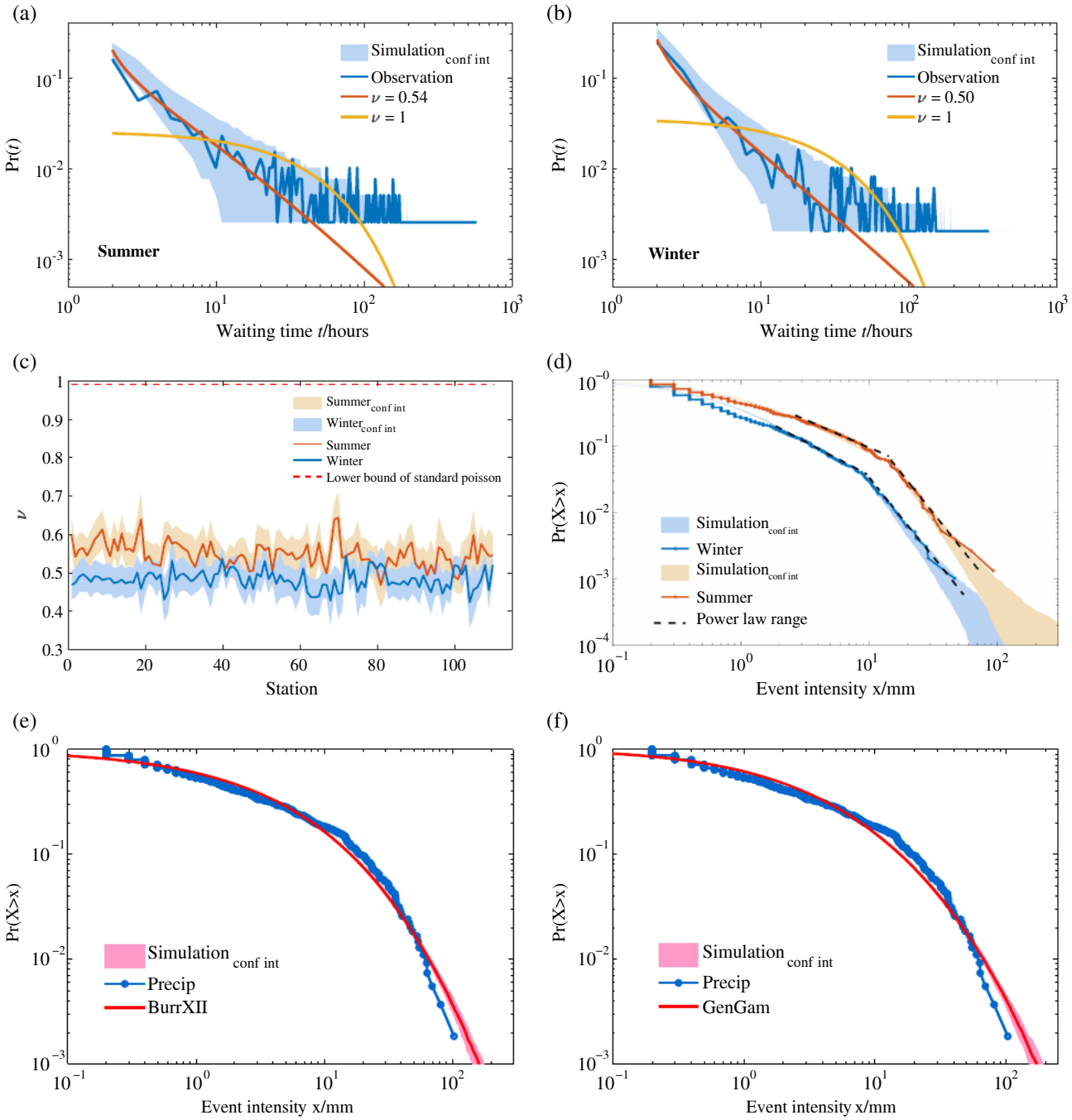

FIGURE 2 Waiting time distribution in (a) summer and (b) winter for the period 2008–2017 versus the waiting time duration (blue line). The blue shading denotes the area of the fractional Poisson process (FPP; red line) which is significant at the 1% confidence level. for comparison, a standard Poisson process, which yields an exponentially distributed waiting time, was fitted to the data (yellow line). (c) Fractional parameter ν for all the observation stations together their 95% confidence levels. The red dashed is the lower bound of 95% confidence level of a standard Poisson process. (d) Precipitation event intensity distribution at Versailles station. The shading denotes the area which is significant at the 1% level. (e and f) Precipitation event intensity distribution of Kingston station in winter. The shading denotes the area which is significant at the 1% level [Colour figure can be viewed at wileyonlinelibrary.com]

an example of a typical waiting time distribution. Versailles is located in the eastern part of the US and has a mild climate with plenty of precipitation all year round. The FPP agrees significantly better with the observations than the standard Poisson process (Figure 2a,b). The fractional parameter ν is 0.54 in summer and 0.50 in winter. By generating 1,000 surrogate waiting time series using the FPP, we see that the empirical waiting time distribution is included at the 99% confidence bound. The flat frequency for longer dry spells is due to the limited samples.

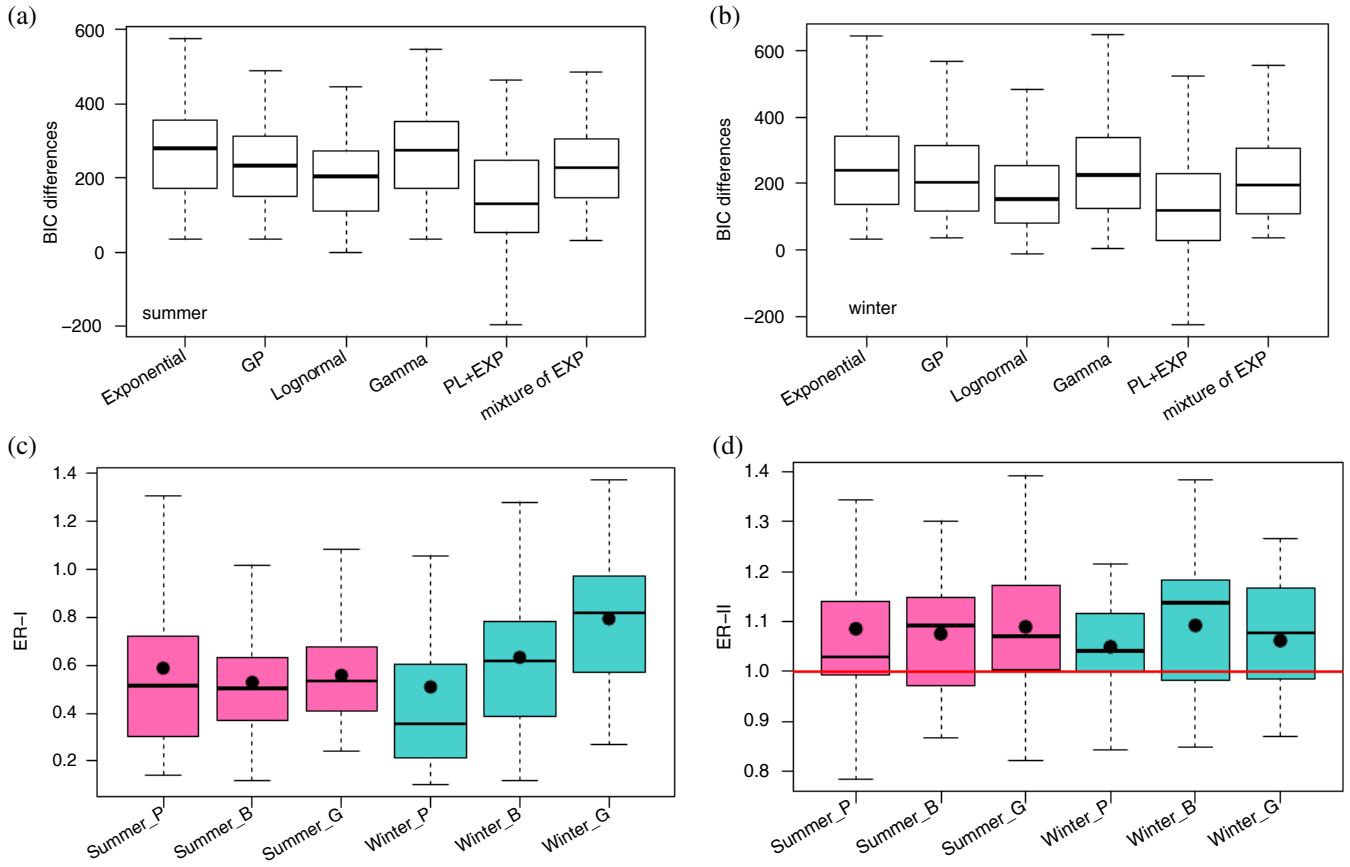

FIGURE 3 BIC differences between the fits of the combined generalized Pareto distribution and a power-law distribution (GP + PL) and some other typically used distributions (exponential, generalized Pareto, lognormal, gamma), and combinations of distributions (power-law with exponential tail, mixture of two exponentials) for all observation stations in summer (a) and winter (b). Positive value means BIC of other distribution is higher than BIC of GP + PL. (c and d) Box plots of error measurement that evaluates the fitting performance of the GP + PL (P), BurrXII (B) and GenGam (g) distributions in the summer and winter seasons. Black points are mean values [Colour figure can be viewed at wileyonlinelibrary.com]

Similar results are also found at all other stations. The fractional parameter ν of the waiting time is different from 1 in both summer and winter (Figure 2c). The mean values are 0.55 in summer and 0.48 in winter. In order to overcome the bias caused by limited samples, we also plot the uncertainties of ν. For all the stations, the waiting times of hourly precipitation events are obviously not exponentially distributed, since ν is significantly smaller than 1. Compared with exponential distributions, there are more short and long dry spells and fewer medium dry spells in the hourly precipitation event series, which can be better captured by a fractional Poisson process. Thus, the occurrence of hourly precipitation events can be significantly better described by a fractional Poisson process than by the typically used standard Poisson process.

3.1.2 | Precipitation intensity results

The precipitation event intensity distribution at Versailles station and the two-distribution model, a GPD for the bulk precipitation and a power-law for the large events are shown in Figure 2d. On the range of more than 2 mm, the observation fits well with the two-distribution model and lies inside the 99% uncertainty bounds.

The probability distribution for large and extreme events is power-law distributed, with the lower bound (x_{min}) of 15.9 mm in summer and 10.2 mm in winter. The slopes are 3.34 and 3.17 respectively.

On the intensity range smaller than $x_{\min}$, the bulk precipitation also decays as a power-law. The two power-law ranges have been marked in Figure 2d. The intensity distribution is not dropping smoothly from the bulk intensity distribution, but has an abrupt break ($x_{\min}$). The positive shape parameter of the GPD for the bulk precipitation also indicates that the second power-law range exists. This explains why the combination of GP and Power-law distributions is necessary for the intensity model. Only one power-law range is not enough to model both the bulk and extreme precipitation. One of the advantages of the GP distribution is that it can generate both exponential and power-law tails for the

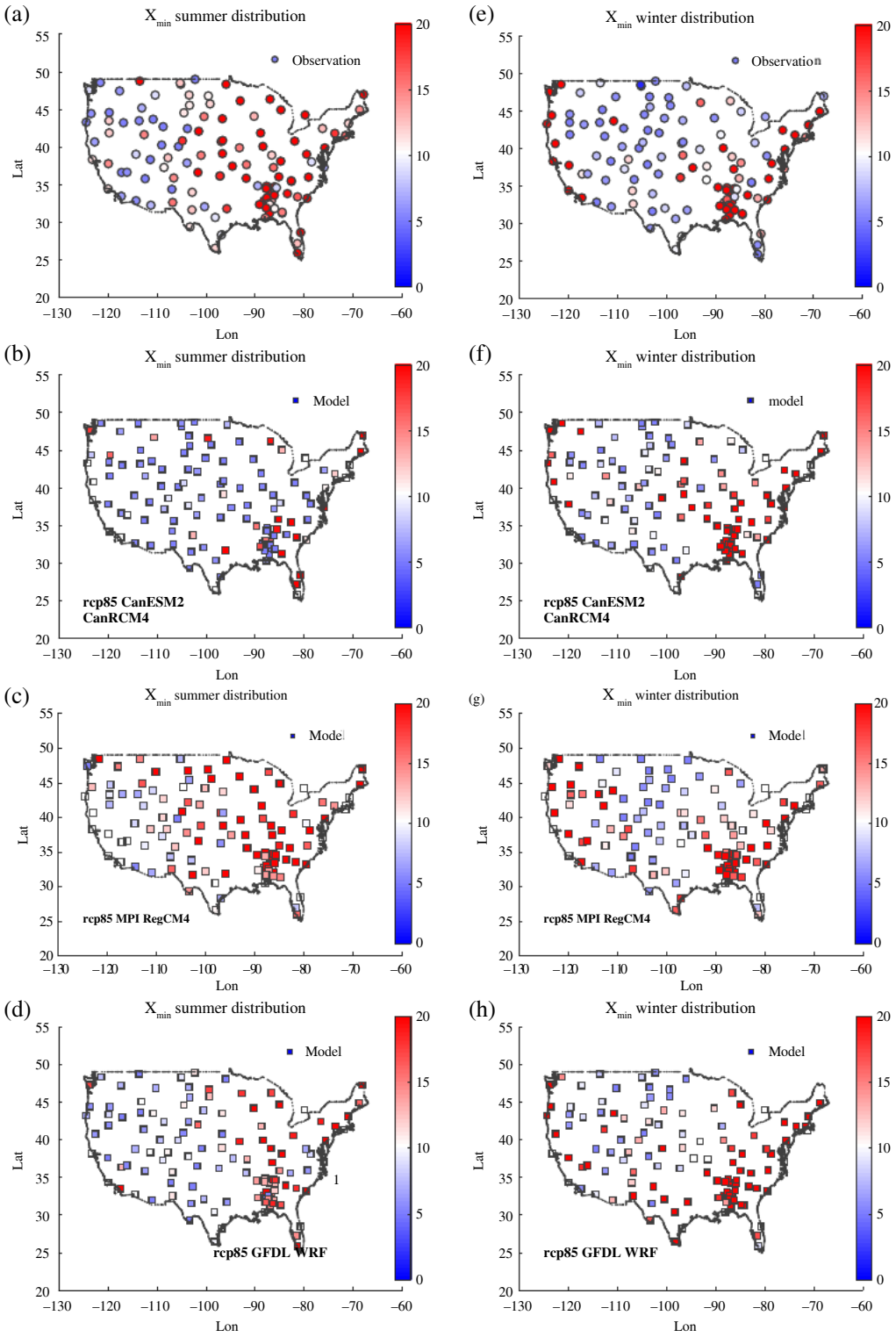

FIGURE 4 Geographical distribution of the upper bound of the power-law tail (x_{min}) in summer and winter of observation (circle dots in a and e) and rcp85 CanESM2-CanRCM4 model (square dots in b and f), rcp85 MPI-RegCM4 model (c and g) and rcp85 GFDL WRF (d and h) [Colour figure can be viewed at wileyonlinelibrary.com]

bulk intensity; the functional form of the GP decay is given by the sign of the shape parameter. In some stations the tail of the bulk precipitation is also power-law distributed and the GP distribution can fit well such stations.

Figure 2e,f shows an additional example of a precipitation intensity distribution based on data of the Kingston station (−71.54 E, 41.48 N) and how it is fitted by the Burr XII and GenGam distributions in the winter season. We select

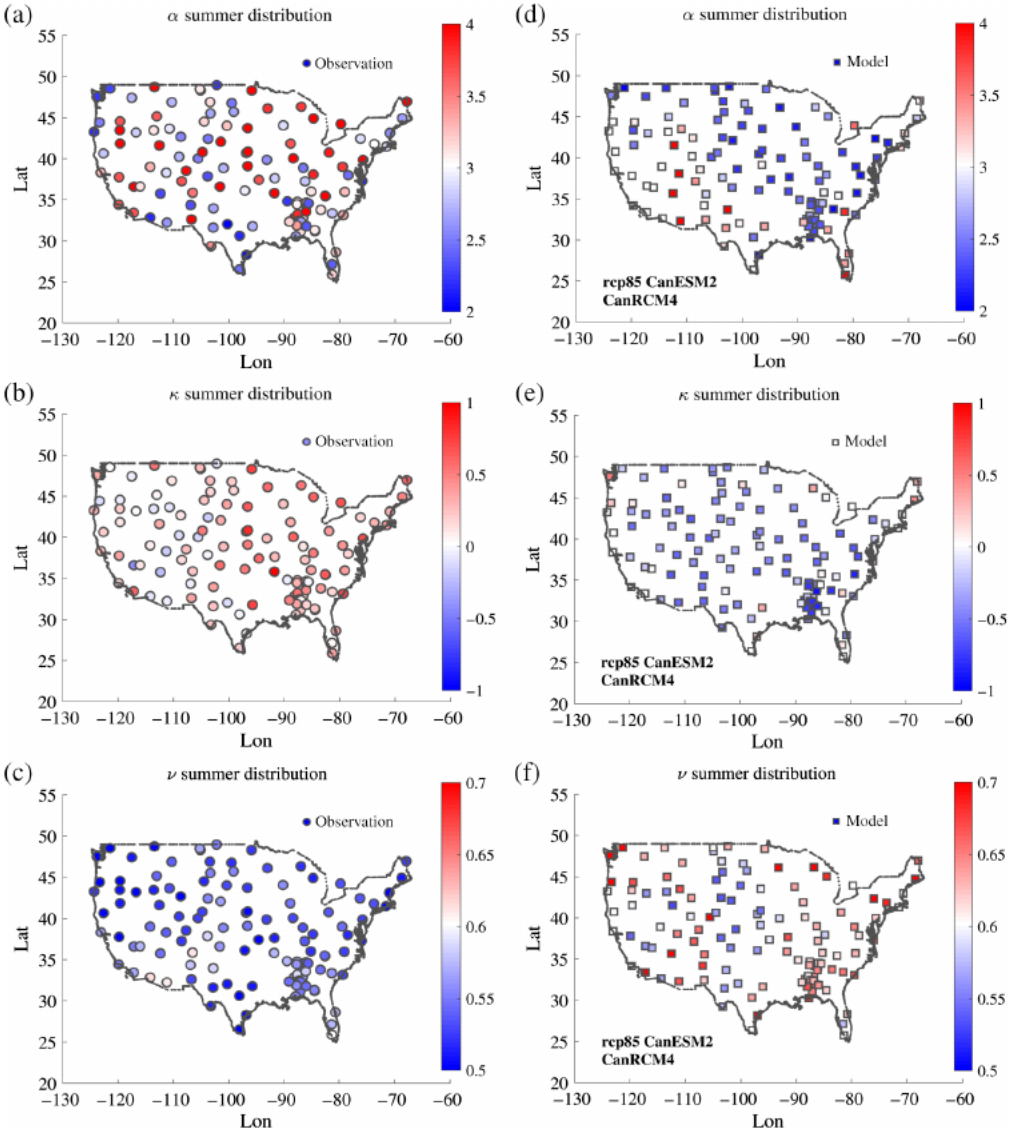

FIGURE 5 Geographical distribution of scaling parameter of power-law tail (α), shape parameter(κ) and fractional Poisson parameter (ν) in summer of observation (circle dots in a, b and c) and rcp85 CanESM2-CanRCM4 model (square dots in d, e and f) [Colour figure can be viewed at wileyonlinelibrary.com]

this station because it can be fitted by both the BurrXII and GenGam distributions. However, we find that there are two different power-law ranges in the intensity distribution and both the BurrXII and GenGam distributions cannot well reproduce them, which leads to an overestimation on the probability of extremes. This suggests that the combination of GPD and a Power-law distribution provides a more accurate and appropriate fit.

We fit all the station data with different classical distributions and find that for most stations a combination of a GPD and a power-law gives the best fit by minimizing BIC. Figure 3a,b shows the BIC difference between the fitting of GP + PL and different typical distributions ($\Delta BIC = BIC_{other\ dsitribution} - BIC_{GP+PL}$). We also get similar results from the AIC calculation. Nearly 90% of the stations in summer and 85% of stations in winter show that the combination of a GP and a Power-law distribution is the best fit, while the remaining 10% are best described by an exponential distribution for the bulk and a power-law distribution for the extremes. The stations which are not fitted best by the GP and Power-law distribute randomly over the United States. As we have shown before, the combination of GP and Power-law distribution is necessary to represent two different power-law ranges of precipitation intensity.

Ninty-eight stations in summer and 104 stations in winter can be well fitted by BurrXII distributions, according to the L-area of the BurrXII distribution. According to the L-area of GenGam distributions, 76 stations in summer and 34 stations in winter can be well fitted by it (not shown). Figure 3c,d show the performance of the fitting for the whole intensity range, quantified by ER-I (Figure 3c) and extreme intensities, quantified by ER-II (Figure 3d). In Figure 3c, the median values of the GP + PL and BurrXII distributions are similar in summer, but with a larger standard deviation for GP + PL. In winter, the GP + PL combination performs much better than the other two distributions. On the fitting for the

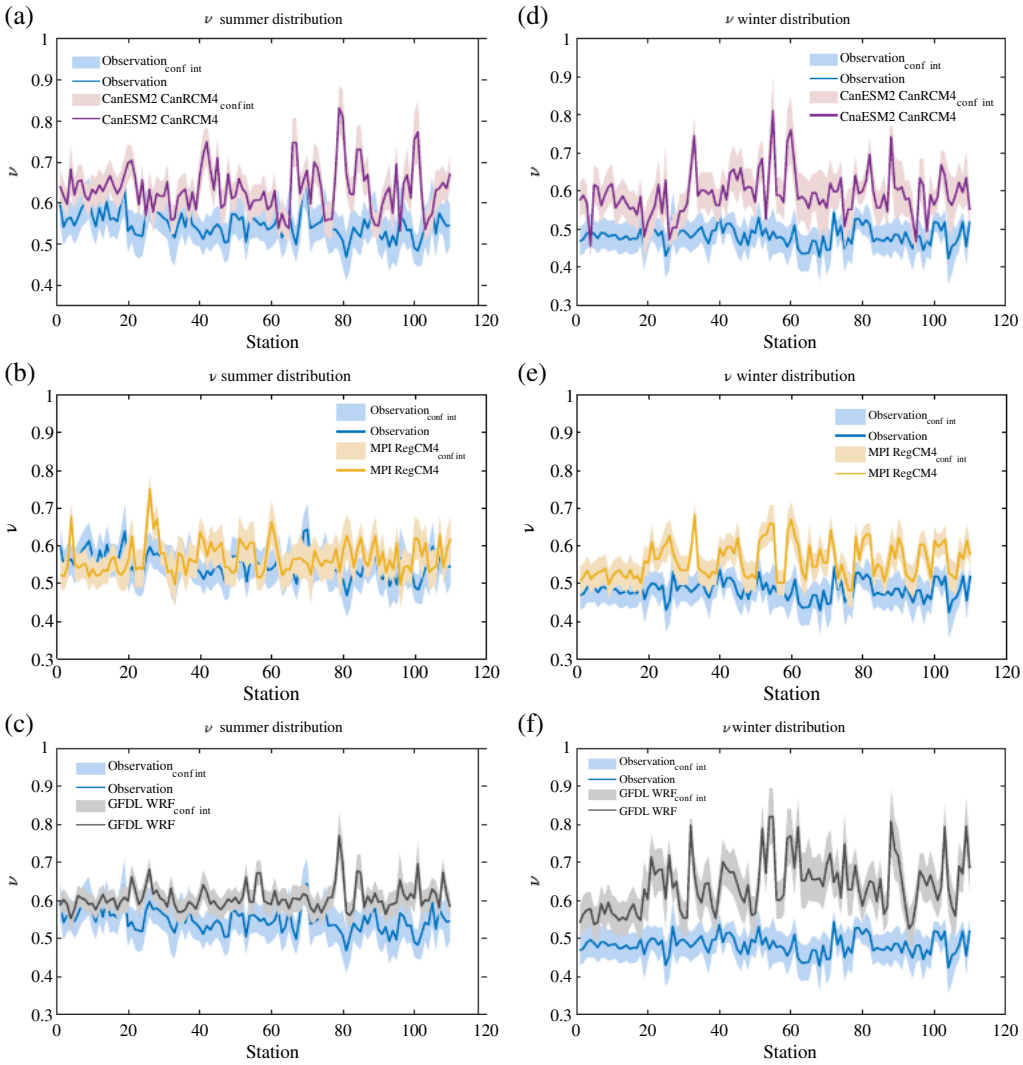

FIGURE 6 Fractional Poisson parameter ν for all observation stations and the closest grid points in CanESM2-CanRCM4 (a and d), MPI-RegCM4 (b and e) and GFDL-WRF (c and f) in summer and winter. The uncertainty of the parameters is indicated by the shading [Colour figure can be viewed at wileyonlinelibrary.com]

extremes (Figure 3d), the median and mean values of ER-II are higher than 1 in both summer and winter, indicating the 99% quantile of intensities are overestimated. ER-II measures of the three distributions are similar in summer, but in winter, ER-IIs of GP + PL are closer to 1. Overall, the three distributions perform similarly in the summer season, but the GP + PL behaves best in the winter season. Another serious problem is that both the BurrXII and GenGam distributions have limiting conditions (e.g., Weibull and Pareto type I) so that neither of them can fit all of the hourly precipitation event intensities. The combination of GP and PL is able to provide a much easier and effective way for intensity modelling.

We fit all the station data with a power-law for the heavy precipitation intensities and a GPD for the bulk intensity and find the two power-law ranges vary with geographic location and season. The value of the lower bound of the tail slope range ($x_{\min}$) reveals significant changes in the western and eastern United States. In summer, a gradient of the lower bound of the power-law tail ($x_{\min}$) exists across the United States, with $x_{\min}$ values increasing toward the eastern United States (Figure 4a). The power-law tail starts from around 8 mm in the west and 15 mm in the east. In winter, most of the larger $x_{\min}$ are located in the southeast and a narrow western part (Figure 4e). The spatial characters of $x_{\min}$ are similar with the heavy precipitation intensity distribution (Hitchens *et al.*, 2013). The scaling parameter α is between 2 and 4 in both summer and winter (Figure 5a,d). The mean value of the scaling parameter is around 3. It is in agreement with De Lima and Grasman (1999), who estimated that $\alpha \approx 3$ with 15-min rainfall data in Portugal, and Tessier *et al.* (1996) who found $\alpha = 3.6$ for the daily rainfall accumulation in France. It should also be mentioned that Olsson (1995) obtained α greater than 2 for 8-min rainfall accumulation and Fraedrich and Larnder (1993) obtained $\alpha = 1.7$ with

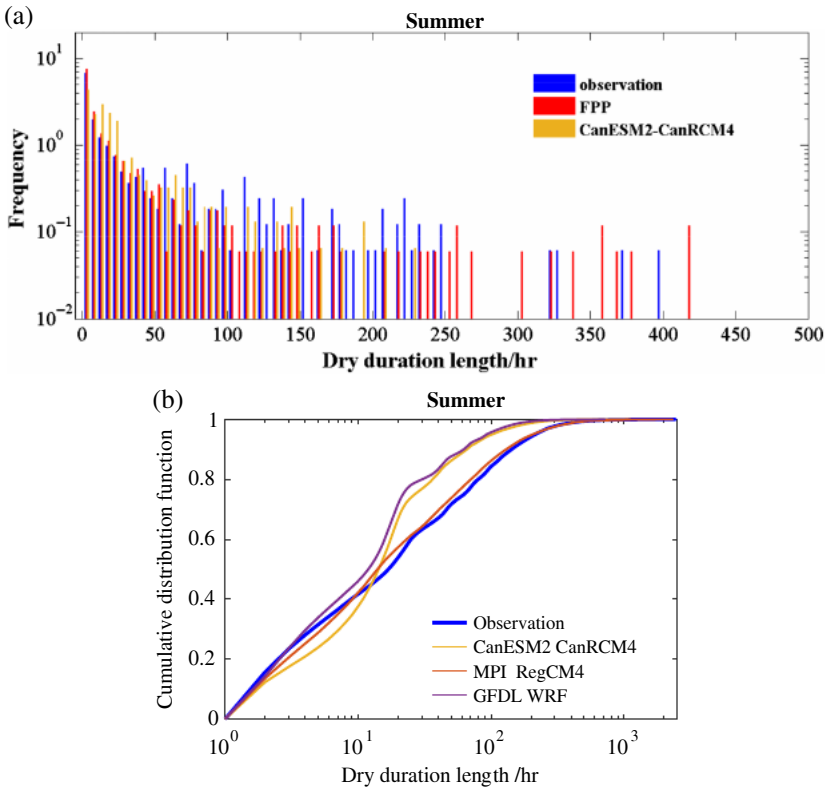

FIGURE 7 (a) Frequency distribution of dry spells duration at Salem station (91.92 W, 37.63 N) of observations, FPP simulation and CanESM2-CanRCM4 model output in summer. (b) Cumulative distribution function of dry spells duration aggregated over all the stations in summer [Colour figure can be viewed at wileyonlinelibrary.com]

1-min rainfall in Germany. It is still unknown whether the variations of the slope estimation are due to the properties of extreme events or the sensitivity of the instruments.

For the bulk precipitation, which is characterized by the GP distribution, most of the shape parameters (κ) of the GP distribution are positive, with 90 in summer and 104 in winter out of 110 stations in total (Figures 5b). The mean values of the shape parameters is 0.34 in summer and 0.49 in winter. A positive shape parameter means, that the tail of the bulk precipitation decreases also as a power-law.

3.2 | Regional climate model precipitation analysis

3.2.1 | Waiting time comparison

In order to better evaluate whether the regional climate model output can capture the characteristics of the observed precipitation, we show the comparison between observation locations and the closest grid point in the form of a line chart. In this way, the uncertainty of each parameter is also considered for comparison.

The mean values and uncertainties of the fractional parameters of the regional climate models are shown in Figure 6. In summer, MPI-RegCM4 behaves better than the other climate models. The parameters are close to the observations in most parts of the United States (Figure 6b). The mean value of ν is 0.57, while the observation mean value is 0.55. The fractional parameter ν of the other regional climate models is significantly overestimated from the observations in most locations (Figures 6a, 5f and 6c), with a mean value of 0.63 in CanESM2-CanRCM4 and 0.61 in GFDL-WRF. The larger exponents mean the waiting time is closer to an exponential distribution, which means the regional climate models generate more medium length dry spells, but lack the ability to generate long dry spells. In winter, none of the climate models represent the fractional parameter well (Figure 6d–f), with mean value 0.64 in CanESM2-CanRCM4, 0.62 in MPI-RegCM4 and 0.59 in GFDL-WRF. All three regional climate models overestimate fractional parameters significantly in most locations.

In order to illustrate the waiting time differences between the observations and regional climate model output more intuitively, we show an example for one particular location, Salem station (91.92 W, 37.63 N), in Figure 7a and the cumulative distribution function for dry spells aggregated over all stations is displayed in Figure 7b. In Figure 7a it can be seen that the CanESM2-CanRCM4 model output generates more medium dry spells (10–50 hr), but lacks the ability to produce longer dry spells, especially the number of dry spells longer than 200 hr. While the waiting times generated by the FPP are able to reproduce longer dry spells and better fit the observation, compared with the CanESM2-CanRCM4 model. Figure 7b shows the cumulative distribution function of dry spells at all locations. We can see that the dry spells obtained from MPI-RegCM4 are

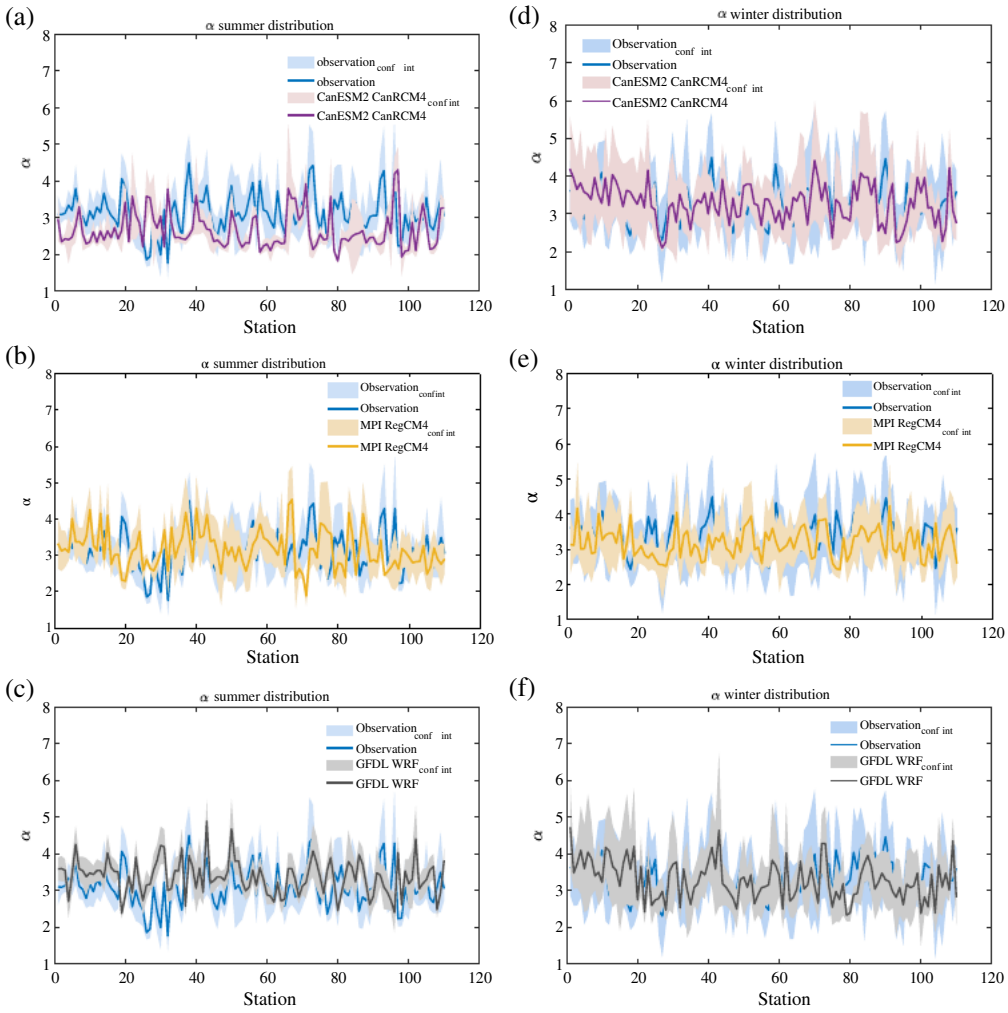

FIGURE 8 α parameter for all observation stations and the closest grid points in CanESM2-CanRCM4 (a and d), MPI-RegCM4 (b and e) and GFDL-WRF (c and f) in summer and winter. The uncertainty of the parameters is indicated shading [Colour figure can be viewed at wileyonlinelibrary.com]

more similar with the observation, consistent with the results we got from the fractional Poisson parameter analysis. The other two models, especially CanESM2-CanRCM4, show a large deviation from the observation. The 80th and 90th quantiles of dry spells of CanESM2-CanRCM4 and GFDL-WRF are both severely underestimated compared with the observation.

3.2.2 | Precipitation intensity comparison

The three used regional climate models behave differently in representing the power-law ranges of precipitation intensities (Figures 4, 5, 8, 9). On the power-law range for large intensities in summer, MPI-RegCM4 is able to capture the geographical differences of $x_{\min}$ in the western and eastern part compared to the other two models (Figure 4c). GFDL-WRF can characterize the lower bound values in the western part well, but underestimates the lower bounds in some places in the east (Figure 4d). CanESM2-CanRCM4 behaves the worst in terms of the geographical distribution of intensities. It underestimates the power-law tail boundary ($x_{\min}$) and does not present the distribution differences between the west and east, as compared with the observations (Figure 4b). In order to quantitatively compare the differences at each location, we compute the mean deviation from the observations $\left(\sqrt{\frac{1}{n}\sum_{i=1}^{i=n}\left(x_{\min\,\mathrm{RCM},\,i}-x_{\min\,\mathrm{Obs},\,i}\right)^2}\right)$. GFDL-WRF can best reproduce the values of $x_{\min}$, with the mean deviation around 10 mm. While the deviations of MPI-RegCM4 and CanESM2-CanRCM4 are 14 and 13 mm. In winter, all of the three regional climate models simulate good lower bounds of the power-law tail in the southeast. Only CanESM2-CanRCM4 characterizes well the spatial differences between the western coastal and central part (Figure 4f). MPI-RegRCM4 overestimated some grids in the west. Among them, the CanESM2-CanRCM4 can best reproduce the magnitude, with the minimum mean deviation around 10 mm, while the deviation of MPI-RegCM4 and GFDL-WRF are about 14 and 15 mm. Thus, in winter, CanESM2-CanRCM4 can best reproduce both the geographical distribution and the values of the lower bounds of the power-law range for large events.

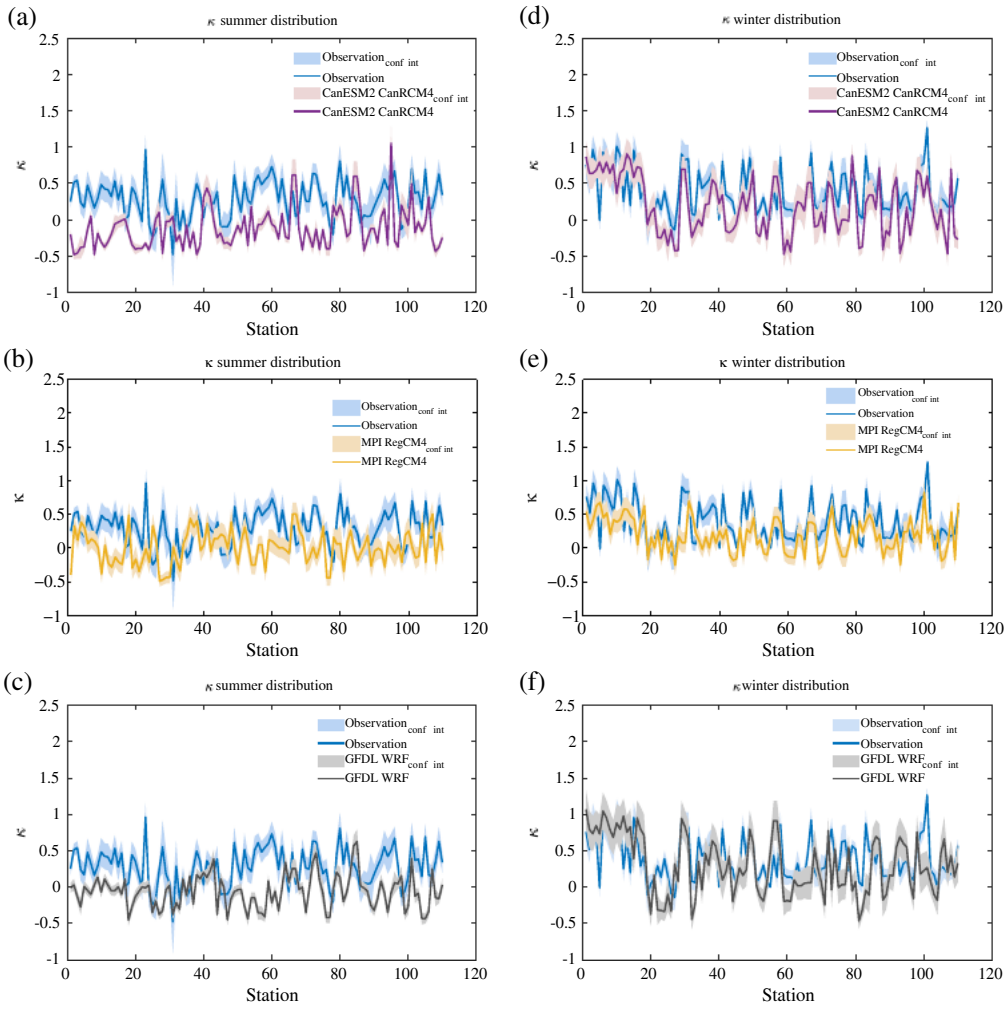

FIGURE 9 κ parameter for all observation stations and the closest grid points in CanESM2-CanRCM4 (a and d), MPI-RegCM4 (b and e) and GFDL-WRF (c and f) in summer and winter. The uncertainty of the parameters is indicated by shading [Colour figure can be viewed at wileyonlinelibrary.com]

The mean values of the scaling parameter α in MPI-RegCM4 ($\hat{\alpha}=2.94$) and GFDL-WRF ($\hat{\alpha}=3.07$) match better with the observations ($\hat{\alpha}=3.01$) in summer (Figure 8b,c). This indicates that the regional climate models can roughly capture the slope of the power-law distribution of the heavy precipitation intensities, while CanESM2-CanRCM4 ($\hat{\alpha}=2.72$) shows an underestimation of α (Figure 8a). In winter, there is a larger uncertainty of the scaling parameters. That may be due to fewer heavy precipitation events occurring in winter (Figure 8d–f).

For the bulk precipitation, the shape parameter of the climate models are underestimated in summer. This is especially the case for CanESM2-CanRCM4 ($\hat{\kappa}=-0.31$) and GFDL-WRF ($\hat{\kappa}=-0.10$) which are displayed in Figure 9a–c. The shape parameter in most of the grid points in CanESM2-CanRCM4 (70/110) and GFDL-WRF (44/110) are negative. That indicates that CanESM2-CanRCM4 and GFDL-WRF cannot characterize the second power-law range on a portion of grid points. In winter, the κ parameter in many grid points of the regional climate models increase and become greater than zero. The mean values of the κ parameter are 0.28, 0.27 and 0.34 for CanESM2-CanRCM4, MPI-RegCM4, GFDL-WRF compared with 0.49 for the observations.

4 | DISCUSSION

Non-exponential distributions are of general interest, as they imply possible nonlinear dynamics of the underlying dynamical processes. Here we analyse the non-exponential distributions of dry spells and intensity of higher-frequency precipitation records because they can provide finer temporal structures of precipitation and can help us to better understand precipitation occurrence.

The Poisson process is one of the most important stochastic processes, which are widely applied to describe the arrival and inter-arrival times of events (Rodriguez-Iturbe *et al.*, 1987; Onof *et al.*, 2000). Independence of the past is an intrinsic property of the standard Poisson Process that leads to exponentially distributed waiting times (Cowpertwait *et al.*, 1996; Olsson and Burlando, 2002). We find that the standard Poisson process cannot well describe the waiting time distributions of hourly precipitation. Our results show that a

fractional Poisson process is more appropriate to model the precipitation occurrence. How the waiting time deviates from an exponential distribution is quantified by the fractional parameter ν. The fractional parameter is also related to power-law exponents. As the FPP function shows, when $t \to \infty$, $\psi(t) = \frac{1}{\mu t^{\nu+1}}$ (Laskin, 2003). When we estimate ν throughout the whole year and calculate the power-law exponent of the waiting time, the mean power law exponent is $\alpha = 1.50 \pm 0.02$. The results are consistent with the ones obtained from Peters *et al.* (2001). The fractional parameter can also quantify the correlation of the return times. In Blender *et al.* (2015) the fractional Poisson process is used to explain the non-exponential return time distribution of vorticity extremes. It has been shown that the fractional parameter ν, which is close to the Weibull shape parameter k, has a relationship with the autocorrelation exponent γ and fluctuation exponent α calculated by detrended fluctuation analysis, $\nu \approx k \approx \gamma = 2 - 2\alpha$.

We find that there are two power-law ranges over the intensity distribution, one is displayed by the form $P(X > x) \sim x^{-\alpha}$, $x > x_{\min}$, one is characterized by the GP distribution. The two power-law ranges of precipitation intensity is consistent with previous work by Fraedrich and Larnder (1993) and Andrade *et al.* (1998). They put forward the idea that the two power-law ranges are a reflection of different scaling regimes of precipitation. It has been widely accepted that precipitation exhibits different scaling regimes which are closely associated with different precipitation systems (Tessier *et al.*, 1996; Olsson and Burlando, 2002; Mascaro *et al.*, 2013). In particular, when the precipitation series is transformed to the frequency domain, the energy $E(f)$ versus the frequency f is linked as a power-law, $E(f) \sim f^{-\alpha}$. Two different slopes can be found, which represent different scaling behaviours of convective storms and frontal systems in the frequency domain (Mascaro *et al.*, 2013). Here, similar results are also found in the amplitude domain. So the two different power-law range might present different scaling regimes of precipitation. One hypothesis is that the two scaling regimes are associated with large-scale stratiform and convective precipitation events, respectively. However, a full explanation for the break in the distribution is still needed and part of our future research.

Regional climate models are used to study the impact of climate change and other hydrological process, such as groundwater reserves (Gao *et al.*, 2006; Rinke *et al.*, 2008; Goderniaux *et al.*, 2011). So the capability of regional climate models in reproducing statistics of precipitation, especially for large events are quite important. We evaluated three RCMs and show that some cannot well reproduce the statistics of hourly precipitation events. Whether it is due to the driving GCMs or dynamical down-scaling is an open research question. Better bias correction procedures are still needed before these models can be used for policy advise.

5 | CONCLUSIONS

In this study we addressed three main research questions:

1. What is the optimal waiting time distribution for hourly precipitation events? Our results show that the observed waiting times between precipitation events in the United States are significantly better characterized by a fractional Poisson process than the typically used standard Poisson process.
2. How best to model the intensity distribution of hourly precipitation? We provide robust evidence that the hourly precipitation intensity can be better described by a combination of two distinct distributions: (a) GPD for the small and bulk precipitation intensities and (b) a power-law distribution for the large and extreme intensities. This combination reproduces the intensity statistics significantly better when compared with other typically used distributions.
3. How well do regional climate models reproduce hourly precipitation observations? Our results provide quantitative evidence that MPI-RegCM4 can well reproduce the waiting times of the hourly precipitation events in summer but not in winter. The CanESM2-CanRCM4 and GFDL-WRF regional models have shortcomings in representing the non-exponential waiting times in both seasons. More specifically, the regional climate models generate more short- and medium-length spells, but lack the capability in producing the long dry spells. Our results provide quantitative evidence that the MPI-RegCM4 captures much of the two power-law intensity ranges in summer and CanESM2-CanRCM4, GFDL-WRF behave better in winter. The good simulations of the two power-law ranges will provide us with a more accurate recurrence prediction of large magnitude events. This is a major potential pitfall when using future climate projections for climate change impact assessment.

Typically, systems exhibiting persistence (Hurst effect) have power-law distributed waiting times (Bunde *et al.*, 2008; Franzke *et al.*, 2015). One example is that the persistence of surface wind speeds leads to clustered extreme events (Franzke, 2013). So a possible reason for the non-exponential waiting times is persistent regime behaviour (Franzke *et al.*, 2015). This would imply that the regional climate models have deficiencies in reproducing the observed regime behaviour over the United States (e.g., Roller *et al.*, 2016). Whether this is due to deficiencies in regime behaviour over the United

States in the driving GCMs or due to the dynamical downscaling is an open research question.

ACKNOWLEDGMENTS

We thank three anonymous reviewers whose comments help to improve this paper. L.Y. acknowledges funding by the Chinese Scholarship Council. C.F. was supported by the collaborative research centre TRR181 sponsored by the Deutsche Forschungsgemeinschaft (DFG German research Foundation) – Project number 274762653. Z.T. was supported by the National Natural Science Foundation of China (41475048, 41675049).The hourly precipitation dataset can be obtained from the website https://www.ncdc.noaa.gov/crn/. Regional climate model output can be obtained at http://na-cordex.org.

ORCID

Lichao Yang https://orcid.org/0000-0001-5124-3406

REFERENCES

Andrade, R.F.S., Schellnhuber, H. and Claussen, M. (1998) Analysis of rainfall records: possible relation to self-organized criticality. *Physica A: Statistical Mechanics and its Applications*, 254(3–4), 557–568.

Bak, P., Tang, C. and Wiesenfeld, K. (1988) Self-organized criticality. *Physical Review A*, 38(1), 364.

Berg, P., Moseley, C. and Haerter, J.O. (2013) Strong increase in convective precipitation in response to higher temperatures. *Nature Geoscience*, 6(3), 181.

Bernardara, P., De Michele, C. and Rosso, R. (2007) A simple model of rain in time: an alternating renewal process of wet and dry states with a fractional (non-Gaussian) rain intensity. *Atmospheric Research*, 84(4), 291–301.

Blender, R., Raible, C. and Lunkeit, F. (2015) Non-exponential return time distributions for vorticity extremes explained by fractional poisson processes. *Quarterly Journal of the Royal Meteorological Society*, 141(686), 249–257.

Buishand, T. (1978) Some remarks on the use of daily rainfall models. *Journal of Hydrology*, 36(3–4), 295–308.

Bunde, A., Eichner, J.F., Havlin, S., Kantelhardt, J.W. and Lennartz, S. (2008) Return intervals and extreme events in persistent time series with applications to climate and seismic records. *Reviews of Nonlinear Dynamics and Complexity*, 1(1),111–145.

Cahoy, D. O., Uchaikin, V. V., & Woyczynski, W. A. (2010) Parameter estimation for fractional Poisson processes. *Journal of Statistical Planning and Inference*, 140(11), 3106–3120.

Cai, Z. and Ofterdinger, U. (2016) Analysis of groundwater-level response to rainfall and estimation of annual recharge in fractured hard rock aquifers, NW Ireland. *Journal of Hydrology*, 535, 71–84.

Cavanaugh, N.R., Gershunov, A., Panorska, A.K. and Kozubowski, T. J. (2015) The probability distribution of intense daily precipitation. *Geophysical Research Letters*, 42(5), 1560–1567.

Chan, S.C., Kendon, E.J., Fowler, H.J., Blenkinsop, S., Ferro, C.A. and Stephenson, D.B. (2013) Does increasing the spatial resolution of a regional climate model improve the simulated daily precipitation? *Climate Dynamics*, 41(5–6), 1475–1495.

Clauset, A., Shalizi, C.R. and Newman, M.E. (2009) Power-law distributions in empirical data. *SIAM Review*, 51(4), 661–703.

Cowpertwait, P.S.P., O'Connell, P.E., Metcalfe, A.V. and Mawdsley, J.A. (1996) Stochastic point process modelling of rainfall. II. Regionalisation and disaggregation. *Journal of Hydrology*, 175(1–4), 47–65.

De Lima, M. and Grasman, J. (1999) Multifractal analysis of 15-min and daily rainfall from a semi-arid region in Portugal. *Journal of Hydrology*, 220(1–2), 1–11.

Diaconescu, E.P., Gachon, P., Laprise, R. and Scinocca, J.F. (2016) Evaluation of precipitation indices over North America from various configurations of regional climate models. *Atmosphere-Ocean*, 54(4), 418–439.

Diaconescu, E.P., Mailhot, A., Brown, R. and Chaumont, D. (2018) Evaluation of CORDEX-Arctic daily precipitation and temperature-based climate indices over Canadian Arctic land areas. *Climate Dynamics*, 50(5–6), 2061–2085.

Evans, J. (2011). CORDEX–an international climate downscaling initiative. In *19th International Congress on Modelling and Simulation*, *Perth*, *Australia*, pp. 12–16.

Fraedrich, K. and Larnder, C. (1993) Scaling regimes of composite rainfall time series. *Tellus A: Dynamic Meteorology and Oceanography*, 45(4), 289–298.

Franzke, C.L. (2013) Persistent regimes and extreme events of the North Atlantic atmospheric circulation. *Philosophical Transactions of the Royal Society A: Mathematical, Physical and Engineering Sciences*, 371(1991), 20110471.

Franzke, C.L., Osprey, S.M., Davini, P. and Watkins, N.W. (2015) A dynamical systems explanation of the Hurst effect and atmospheric low-frequency variability. *Scientific Reports*, 5, 9068.

Gao, X., Pal, J.S. and Giorgi, F. (2006) Projected changes in mean and extreme precipitation over the Mediterranean region from a high resolution double nested RCM simulation. *Geophysical Research Letters*, 33(3), 289–305.

Goderniaux, P., Brouyere, S., Blenkinsop, S., Burton, A., Fowler, H.J., Orban, P. and Dassargues, A. (2011) Modeling climate change impacts on groundwater resources using transient stochastic climatic scenarios. *Water Resources Research*, 47(12), W12516.

Haerter, J.O., Eggert, B., Moseley, C., Piani, C. and Berg, P. (2015) Statistical precipitation bias correction of gridded model data using point measurements. *Geophysical Research Letters*, 42(6), 1919–1929.

Hannachi, A. (2014) Intermittency, autoregression and censoring: a first-order AR model for daily precipitation. *Meteorological Applications*, 21(2), 384–397.

Hitchens, N.M., Brooks, H.E. and Schumacher, R.S. (2013) Spatial and temporal characteristics of heavy hourly rainfall in the United States. *Monthly Weather Review*, 141(12), 4564–4575.

Laskin, N. (2003) Fractional poisson process. *Communications in Nonlinear Science and Numerical Simulation*, 8(3–4), 201–213.

Laskin, N. (2009) Some applications of the fractional poisson probability distribution. *Journal of Mathematical Physics*, 50(11), 113513.

Lenderink, G. and Van Meijgaard, E. (2008) Increase in hourly precipitation extremes beyond expectations from temperature changes. *Nature Geoscience*, 1(8), 511.

Lennartsson, J., Baxevani, A. and Chen, D. (2008) Modelling precipitation in Sweden using multiple step Markov chains and a composite model. *Journal of Hydrology*, 363(1–4), 42–59.

Liang, X.-Z., Li, L., Dai, A. and Kunkel, K.E. (2004) Regional climate model simulation of summer precipitation diurnal cycle over the United States. *Geophysical Research Letters*, 31(24), L24208.

Maraun, D., Wetterhall, F., Ireson, A., Chandler, R., Kendon, E., Widmann, M., Brienen, S., Rust, H., Sauter, T., Themeßl, M., et al. (2010) Precipitation downscaling under climate change: recent developments to bridge the gap between dynamical models and the end user. *Reviews of Geophysics*, 48(3), L24208.

Martinez-Villalobos, C. and Neelin, J.D. (2018) Shifts in precipitation accumulation extremes during the warm season over the United States. *Geophysical Research Letters*, 45(16), 8586–8595.

Martynov, A., Laprise, R., Sushama, L., Winger, K., Šeparović, L. and Dugas, B. (2013) Reanalysis-driven climate simulation over CORDEX North America domain using the Canadian regional climate model, version 5: model performance evaluation. *Climate Dynamics*, 41(11–12), 2973–3005.

Mascaro, G., Deidda, R. and Hellies, M. (2013) On the nature of rainfall intermittency as revealed by different metrics and sampling approaches. *Hydrology and Earth System Sciences*, 17(1), 355–369.

Mielke, P.W. and Johnson, E.S. (1974) Some generalized beta distributions of the second kind having desirable application features in hydrology and meteorology. *Water Resources Research*, 10(2), 223–226.

Muschinski, T. and Katz, J. (2013) Trends in hourly rainfall statistics in the United States under a warming climate. *Nature Climate Change*, 3(6), 577.

Olsson, J. (1995) Limits and characteristics of the multifractal behaviour of a high-resolution rainfall time series. *Nonlinear Processes in Geophysics*, 2(1), 23–29.

Olsson, J. and Burlando, P. (2002) Reproduction of temporal scaling by a rectangular pulses rainfall model. *Hydrological Processes*, 16(3), 611–630.

Onof, C., Chandler, R., Kakou, A., Northrop, P., Wheater, H. and Isham, V. (2000) Rainfall modelling using poisson-cluster processes: a review of developments. *Stochastic Environmental Research and Risk Assessment*, 14(6), 384–411.

Papalexiou, S.M. (2018) Unified theory for stochastic modelling of hydroclimatic processes: preserving marginal distributions, correlation structures, and intermittency. *Advances in Water Resources*, 115, 234–252.

Papalexiou, S.M. and Koutsoyiannis, D. (2016) A global survey on the seasonal variation of the marginal distribution of daily precipitation. *Advances in Water Resources*, 94, 131–145.

Papalexiou, S., Koutsoyiannis, D. and Makropoulos, C. (2013) How extreme is extreme? An assessment of daily rainfall distribution tails. *Hydrology and Earth System Sciences*, 17(2), 851–862.

Papalexiou, S.M., AghaKouchak, A. and Foufoula-Georgiou, E. (2018) A diagnostic framework for understanding climatology of tails of hourly precipitation extremes in the United States. *Water Resources Research*, 54(9), 6725–6738.

Paschalis, A., Molnar, P., Fatichi, S. and Burlando, P. (2013) A stochastic model for high-resolution space-time precipitation simulation. *Water Resources Research*, 49(12), 8400–8417.

Pendergrass, A.G. and Knutti, R. (2018) The uneven nature of daily precipitation and its change. *Geophysical Research Letters*, 45(21), 11–980.

Peters, O., Hertlein, C. and Christensen, K. (2001) A complexity view of rainfall. *Physical Review Letters*, 88(1), 018701.

Rinke, A., Kuhry, P. and Dethloff, K. (2008) Importance of a soil organic layer for Arctic climate: a sensitivity study with an Arctic RCM. *Geophysical Research Letters*, 35(13), L13709.

Rodriguez-Iturbe, I., Cox, D.R. and Isham, V. (1987) Some models for rainfall based on stochastic point processes. *Proceedings of the Royal Society of London A*, 410(1839), 269–288.

Roller, C.D., Qian, J.-H., Agel, L., Barlow, M. and Moron, V. (2016) Winter weather regimes in the Northeast United States. *Journal of Climate*, 29(8), 2963–2980.

Salvadori, G. and De Michele, C. (2001) From generalized Pareto to extreme values law: scaling properties and derived features. *Journal of Geophysical Research-Atmospheres*, 106(D20), 24063–24070.

Saxena, R., Mathai, A. and Haubold, H. (2002) On fractional kinetic equations. *Astrophysics and Space Science*, 282(1), 281–287.

Shao, Q. (2004) Notes on maximum likelihood estimation for the three-parameter Burr XII distribution. *Computational Statistics & Data Analysis*, 45(3), 675–687.

Swift, L.W., Jr. and Schreuder, H.T. (1981) Fitting daily precipitation amounts using the SB distribution. *Monthly Weather Review*, 109 (12), 2535–2540.

Tessier, Y., Lovejoy, S., Hubert, P., Schertzer, D. and Pecknold, S. (1996) Multifractal analysis and modeling of rainfall and river flows and scaling, causal transfer functions. *Journal of Geophysical Research-Atmospheres*, 101(D21), 26427–26440.

Wheater, H.S. (2006) Flood hazard and management: a UKperspective. *Philosophical Transactions of the Royal Society of London A: Mathematical, Physical and Engineering Sciences*, 364(1845), 2135–2145.

Wilks, D.S. and Wilby, R.L. (1999) The weather generation game: a review of stochastic weather models. *Progress in Physical Geography*, 23(3), 329–357.

Wilson, P. and Toumi, R. (2005) A fundamental probability distribution for heavy rainfall. *Geophysical Research Letters*, 32(14), L14812.

Woolhiser, D.A., et al. (1982) Stochastic daily precipitation models: 1. A comparison of occurrence processes. *Water Resources Research*, 18(5), 1451–1459.

Xie, F., Nian, D. and Fu, Z. (2019) Differential temporal asymmetry among different temperature variables' daily fluctuations. *Climate Dynamics*, 53(1–2), 585–600.

How to cite this article: Yang L, Franzke CLE, Fu Z. Power-law behaviour of hourly precipitation intensity and dry spell duration over the United States. *Int J Climatol*. 2020;40:2429–2444. https://doi.org/10.1002/joc.6343

APPENDIX. ADDITIONAL COMPARISON WITH OTHER DATASETS

The TD3240 dataset provides hourly precipitation for a network over 7,000 stations across the United States (https://www1.ncdc.noaa.gov/pub/data/cdo/documentation/PRECIP_HLY_documentation.pdf). The records range from 1 year to more than 100 years. However, we decided not to use this dataset because of its poor quality (nearly 20% missing values) and coarse measurement resolution (2.54 mm). Since we are analysing the statistics of hourly precipitation events, a broader intensity range and fewer missing values are quite important. We pick one station from the USCRN dataset and compare it with the closest station of TD3240 as an example. Figure A1 shows intensity distribution of the station in summer and winter season. The two intensity distribution looks similar on the overlapped intensity range. Even though the USCRN dataset is 10 year long, it can well present the intensity distribution. The resolution of TD3240 data set is 2.54 mm, so it cannot provide the intensity information of less than 2.54 mm. Since we analyse the whole range of intensities, not just the extremes, a higher measurement resolution dataset can provide us more information. So we decided to use the 110 stations, 10-year-long high-quality precipitation dataset.

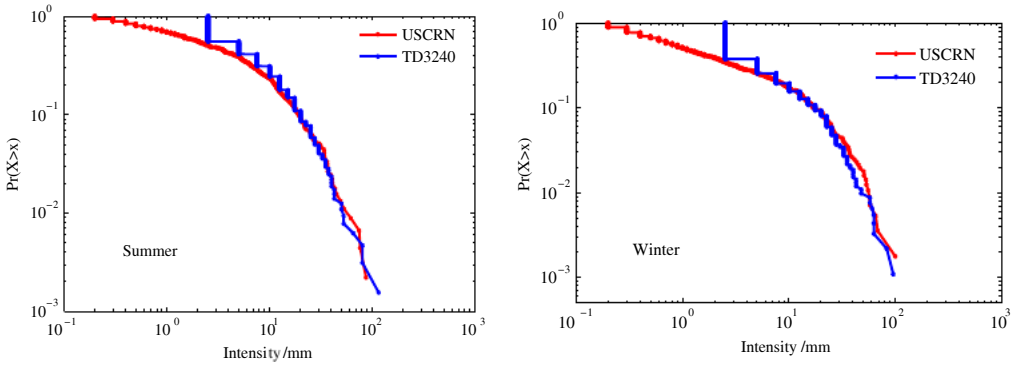

FIGURE A1 Intensity distribution of precipitation event in summer and winter seasons, at two close locations from the two datasets [Colour figure can be viewed at wileyonlinelibrary.com]